Oxygen permeation, thermal and chemical expansion of (La, Sr)(Fe, Ga)O3–δ perovskite membranes

Enrique Juste, Aurélie Julian, G. Etchegoyen, Pierre-Marie Geffroy, Thierry Chartier, N. Richet, P. del Gallo

Oxygen permeation, thermal and chemical expansion of (La, Sr)(Fe, Ga)$O_{3-\delta}$ perovskite membranes

E. JUSTE [1-2], A. JULIAN [1-2], G. ETCHEGOYEN [1-2] , P.M. GEFFROY [1],
T. CHARTIER [1], N. RICHET [2], P. DEL GALLO [2].
[1]SPCTS CNRS, ENSCI, 47 avenue Albert Thomas 87065, Limoges, France
[2]Air Liquide, Centre de Recherche Claude-Delorme 1, chemin de la porte des Loges
Les Loges-en-Josas B.P. 126 – 78354 Jouy-en-Josas Cedex, France

Abstract:

Dense ceramic membranes made from mixed conductors are interesting because of their potential applications for methane conversion into syngas (H_2 CO mixture). Such membranes need to present a low differential dimensional variation between the opposite faces submitted to a large gradient of oxygen partial pressure, in order to minimize mechanical stresses generated through the membrane thickness. Besides, high oxygen permeability is required for high methane reforming rate. $La_{(1-x)}Sr_xFe_{(1-y)}Ga_yO_{3-\delta}$ materials fulfil these two main requirements and were retained as membranes in catalytic membrane reactors (CMR). The variations of expansion and oxygen permeation of $La_{(1-x)}Sr_xFe_{(1-y)}Ga_yO_{3-\delta}$ perovskite materials with the partial substitution of lanthanum and iron cations, temperature and oxygen partial pressure, were studied. For low temperatures (<800°C), the Thermal Expansion Coefficient (TEC) value of $La_{(1-x)}Sr_xFe_{(1-y)}Ga_yO_{3-\delta}$ materials is independent of cation substitution and of oxygen partial pressure in the range tested (10^{-5} to 0.21 atm). For higher temperatures (>800°C), TEC, then dimensional stability of the membrane, and oxygen permeation of $La_{(1-x)}Sr_xFe_{(1-y)}Ga_yO_{3-\delta}$ materials, are significantly affected by Sr content and oxygen partial pressure. Ga has a stabilisation effect on the TEC and has no influence on oxygen permeation flux. A good compromise between dimensional stability and oxygen permeation of materials was found to be $La_{0.7}Sr_{0.3}Fe_{0.7}Ga_{0.3}O_{3-\delta}$ composition.

Keywords: Catalytic Membrane Reactor; Perovskite; Thermal expansion; Chemical expansion; Oxygen permeability

1. Introduction

Ceramic oxides with mixed oxygen-ionic and electronic conductivity have received during the past decades, a great academic and industrial attention for their critical applications in the domain of energy. They are used in high temperature electrochemical reactor systems, like electrodes of solid oxide fuel cells (SOFCs), oxygen pump and membranes for oxygen separation from air and partial oxidation of methane in ceramic membrane reactor (CMR). For this last application, they are typically used at a temperature higher than 700°C to separate selectively oxygen from air and to transport it using the partial pressure gradient of oxygen as driving force without external electrons circuitry. The aim is the reaction of partial oxidation of methane (POM: $CH_4 + ½\ O_2 \rightarrow CO + 2\ H_2$) via a specific catalysis layer to obtain a synthesis gas (mixture of CO and H_2) [1-3]. This synthesis gas or "syngas", is a feedstock for the gas-to-liquid conversion of natural gas to liquid fuels and an intermediate stage in the production of more value–added products such as methanol.

More than twenty years ago, Teraoka et al were the first to study ferrocobaltite materials for their oxygen transport properties [4]. From this time, several potential perovskite-type oxide (ABO_3) materials have been studied, in particular for their oxygen transport properties. For industrial use, a ceramic membrane material must satisfy numerous requirements such as, long term chemical and structural stability at high temperature and under an oxygen partial pressure gradient, a mechanical reliability and a high oxygen permeation rate [5].

The membrane material in a ceramic membrane reactor is exposed on one side to an oxidizing atmosphere and on the other side to a reducing atmosphere. The expansion behaviour of perovskite materials will depend on the oxygen partial pressure and temperature. Indeed, the lattice volume of mixed ionic conductor perovskite will tend to equilibrate with the oxygen partial pressure for a given temperature. Then, the effect of a large oxygen chemical potential gradient through a perovskite membrane reactor can induce mechanical stresses at high temperature because of the differential chemical expansion of the material. In working conditions, these stresses can lead to ceramic membrane failure [1,3,6].

In this context, perovskite like $La_{(1-X)}Sr_XFe_{(1-Y)}Ga_YO_{3-\delta}$ are promising materials for membrane applications due to the dimensional stability at high temperature under oxygen partial pressure gradient [7].

This work is focused on the influence of lanthanum substitution by strontium (X) and iron by gallium (Y) on the thermal expansion and the expansion due to chemical pheneomena of the lattice of $La_{(1-X)}Sr_XFe_{(1-Y)}Ga_YO_{3-\delta}$ with temperature and oxygen partial pressure. Finally, the effect of both substitutions, on oxygen permeation properties, was evaluated on membranes with similar microstructures.

2. Experimental and characterization

2.1 Powders synthesis

$La_{(1-X)}Sr_XFe_{(1-Y)}Ga_YO_{3-\delta}$ powders were synthesized from ultra pure precursors of metal oxides and carbonate, i.e. La_2O_3 (99.99%, Ampere Industrie, France); Fe_2O_3 (99.8%, Socolab, France); Ga_2O_3 (99.99%,Sigma Aldrich Chemical, France) and $SrCO_3$ (99.9, Solvay Atmio E Derivati, France). Powders were prepared by classic solid state reaction as described elsewhere [8]. After weighing the stoechiometry amounts, oxides and carbonate were attrition-milled for 3 hours in ethanol using zirconia media, separated from ball, dried and calcined at 1000°C for 8 hours. After calcination, the synthesized powder was attrition-milled in ethanol, using zirconia media, in order to decrease the mean particule size down to 0.6 µm with a monomodal distribution (laser granulometer, Malvern Instruments Mastersizer 2000).

$La_{(1-X)}Sr_XFe_{(1-Y)}Ga_YO_{3-\delta}$ compositions will be designated by the abbreviation LSFG (1-X)X(1-Y)Y; for instance $La_{0.7}Sr_{0.3}Fe_{0.7}Ga_{0.3}O_{3-\delta}$ is designated LSFG 7373. The various compositions studied are presented in Figure 1.

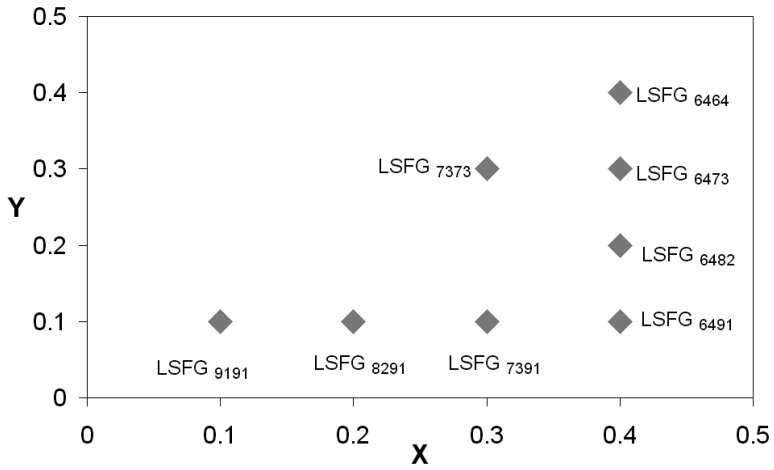

Figure 1 : $La_{(1-X)}Sr_XFe_{(1-Y)}Ga_YO_{3-\delta}$ compositions studied.

2.2 Characterization

Phase crystallographic structures were determined by X-ray diffraction (XRD) using $CuK_{\alpha 1}$ radiation on Debeye-Scherer system. A profile fitting program was used in order to calculate diffraction peak intensities, and positions. A silicium powder was added to LSFG perovskite samples to measure lattice parameters from diffractograms.

Density values of sintered materials were measured using Archimedes method.

For dilatometric characterization, $La_{(1-X)}Sr_XFe_{(1-Y)}Ga_YO_{3-\delta}$ powders were pressed and sintered at 1300°C for 2 hours under 10 % O_2 + 90 % N_2 atmosphere. Relative density values of sintered samples obtained were higher than 95 %. Prior to dilatometric characterization, samples were annealed in atmospheric air (21 % O_2 + 79 % N_2) at 1050°C for 1 hour, with a heating rate of 4°C/min, and then slowly furnace-cooled in order to achieve equilibrium with atmospheric air at room temperature [7]. The sintering atmosphere of samples being different from a dilatometric measurement atmosphere, this annealing step allows to start dilatometric measurement on samples with an oxygen non-stoechiometry in equilibrium with the dilatometric measurement atmosphere. Without this annealing step, the dilatation signal could be masked by the oxygen equilibrium of materials. Dilatometric measurements were performed from room temperature up to 1050°C, with a heating and cooling rate of 4°C/min, under air and nitrogen (Adamel Lhomargy DI-24, France). The annealing step is not necessary for dilatometric measurements performed under nitrogen.

The grain size distribution was determinated from Scanning Electron Microscope micrographs (SEM S-2500, Hitachi) on polished cross sections of membranes. Grain boundaries were previously thermally etched 50°C below their sintering temperature for 12 min. Grain size distributions were calculated using an image analysis software (Aphelion, ADCIS, France) after treatment of about 1000 grains assimilated to spheres.

The oxygen permeation performance was measured on dense membranes shaped by a tape casting process as explained elsewhere [8, 9] using a specific device (Figure 2). A cylindrical dense 1 mm thick membrane was placed between two alumina support tubes, inserted in a vertical tubular furnace and sealed with Pyrex-based glass rings at 1020°C for 30 minutes. After sealing, an oxygen partial pressure gradient is created between the two membrane faces by a flow 100 ml/min synthetic air on the bottom face and argon (200 ml/min) on the upper face. An YSZ-oxygen sensor recorded the oxygen permeation through the membrane in the temperature range 750 to 975°C. The permeating oxygen gas flux through the membrane was defined as follow (1):

$$jO_2 = \frac{C \times F}{S} \times \beta \qquad (1)$$

where: jO_2 is the oxygen permeation flux through the membrane ($Nm^3/m^2/h$); C, the oxygen amount measured (ppm); F, the carrier gas output flow (argon) (m^3/h); S, the membrane effective reacting area (m^2); $S = 2.83.10^{-4} m^2$; and β, the normalization volume coefficient:

$$\beta = \frac{P_{measured} \times T_{(STP)}}{P_{(STP)} \times T_{measured}}$$

with (T(STP) = 298 K and P(STP) = 10^5 Pa).

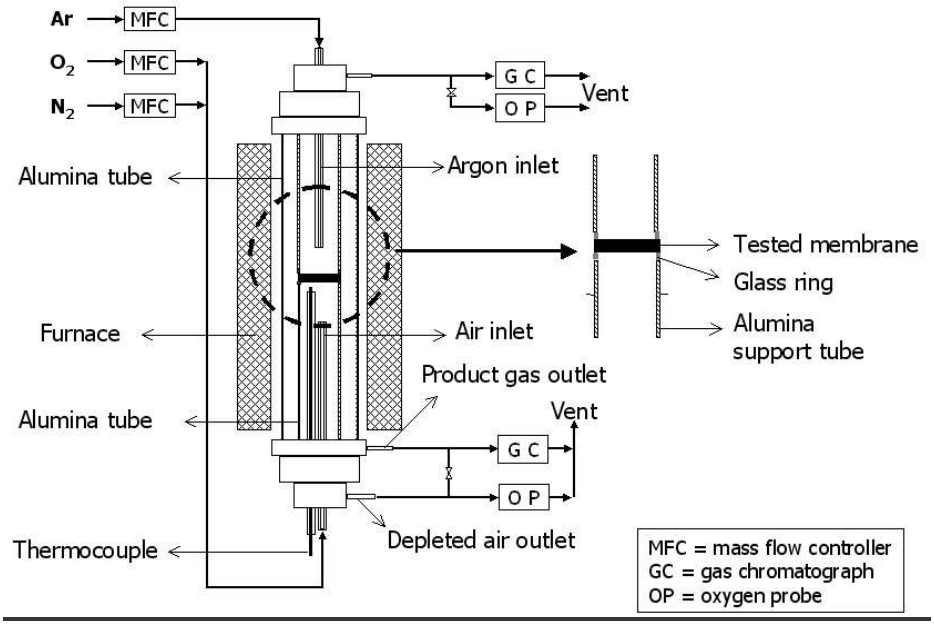

Figure 2 : Schematic diagram of oxygen permeation flux measurements.

3. Results and discussions

3.1 Structural and chemical analysis

The crystallographic phases of the synthesized LSFG powders were identified by XRD (Figure 3). All samples presented a major perovskite phase, with the presence of minor secondary phases. These minor amount phases were identified as La_2O_3, a non reacted precursor part, and $SrFeLaO_4$, an intermediary reaction product. The presence of these minor impurities is mainly due to the synthesis mode of those materials.

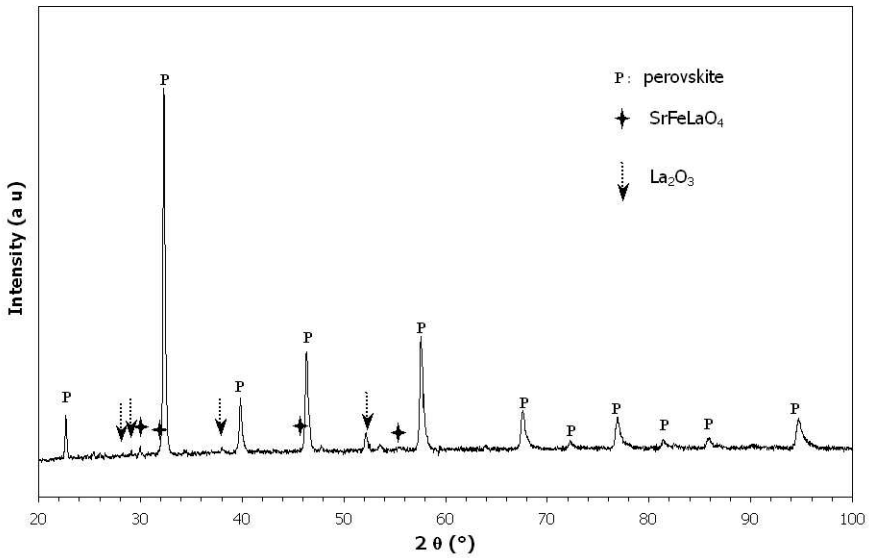

Figure 3 : Example of XRD pattern of $La_{0,8}Sr_{0,2}Fe_{0,9}Ga_{0,1}O_{3-\delta}$.

In order to determine the structural features of sintered membranes and the influences of cation substitutions on the perovskite structure, LSFG samples were calcined at 1300°C for 2 hours under air, then crushed in agate mortar before XRD analysis to obtain a sufficient resolution for lattice parameters measurement. A perovskite structure phase with a rhombohedral symmetry was observed for LSFG 6491 (Table 1). For composition with x = 0.4, from LSFG 6491 to LSFG 6464, the increase of gallium content leads to an evolution of the crystalline symmetry from rhombohedral to cubic and to an expansion of the unit cell volume. The same evolution was observed when strontium content is decreasing from LSFG 6491 to LSFG 9191 (Table 1).

Table 1: Structural evolution of $La_{1-X}Sr_XFe_{1-Y}Ga_YO_{3-\delta}$ with cation substitution.

Materials	Crystalline Symmetry	a (Å)	V (Å^3)	α (°)
$La_{0.6}Sr_{0.4}Fe_{0.9}Ga_{0.1}O_{3-\delta}$	rhombohedral	3.89_1	58.9_1	89.77
$La_{0.6}Sr_{0.4}Fe_{0.6}Ga_{0.4}O_{3-\delta}$	cubic	3.91_5	59.9_9	90.00
$La_{0.9}Sr_{0.1}Fe_{0.9}Ga_{0.1}O_{3-\delta}$	cubic	3.92_3	60.3_9	90.00

3.2 Dilatometric behaviour

Parent ceramics of $La_{1-X}Sr_XFe_{1-Y}Ga_YO_{3-\delta}$ present a singular expansion behaviour as shown on Figure 4. Those singular curves consist of two parts fitted using a linear

model with a slope break around 800°C. A similar behaviour was already reported for perovskite materials, such as $La_{0.3}Sr_{0.7}FeO_{3-\delta}$ or $Sr_{0.85}Ce_{0.15}Fe_{0.8}Co_{0.2}O_{3-\delta}$, etc [5,10,11].

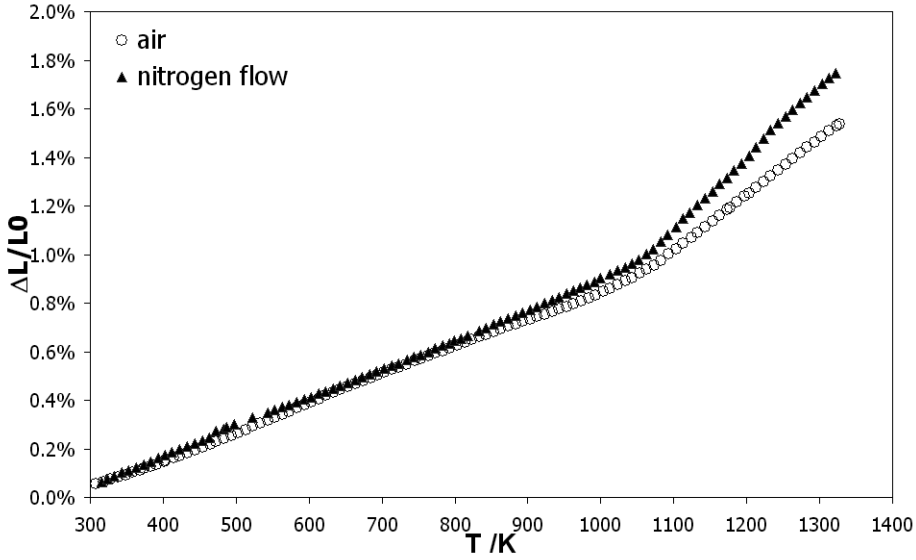

Figure 4 : Dilatometric curves of $La_{0.6}Sr_{0.4}Fe_{0.9}Ga_{0.1}O_{3-\delta}$ ceramic in air (pO_2 = 0.21) and nitrogen ($pO_2 = 5 \times 10^{-6}$).

The apparent Thermal Expansion Coefficient (TEC) is defined as the slope of dilatometric curve. In the low temperature range (20–700°C), the dilatometric behaviour is linear and TEC is almost constant. TEC values of $La_{1-X}Sr_XFe_{1-Y}Ga_YO_{3-\delta}$ compositions are close under air (pO_2 = 0.21 atm) and under nitrogen ($pO_2 = 5 \times 10^{-6}$ atm) within 5% experimental error. But in the high temperature range, between 800–1050°C, firstly the TEC values are markedly larger than those in the low temperature range, and secondly the TEC values under low oxygen partial pressure ($pO_2 = 5 \times 10^{-6}$ atm) are larger than those under air (pO_2 = 0.21 atm). Above 800°C, the TEC can vary with temperature, and a TEC average value is calculated. TEC values measured on $La_{1-X}Sr_XFe_{1-Y}Ga_YO_{3-\delta}$ compositions are summarized in Table 2, under air and nitrogen.

Table 2: Thermal Expansion Coefficient of $La_{1-X}Sr_XFe_{1-Y}Ga_YO_{3-\delta}$ compositions under two oxygen partial pressures (air:pO_2 = 0.21 and nitrogen: $pO_2 = 5x10^{-6}$).

pO_2 = 0.21

Composition	α (10^{-6} °C^{-1}) 20–600°C	α (10^{-6} °C^{-1}) 870–1050°C
LSFG 9191	10.2	13.4
LSFG 8291	8.9	14.8
LSFG 7391	10.8	15.8
LSFG 6491	11.8	23.1
LSFG 7373	11.0	18.5
LSFG 6473	11.4	20.8
LSFG 6464	9.8	19.9
LSFG 6482	11.7	19.2

$pO_2 = 5x10^{-6}$

Composition	α (10^{-6} °C^{-1}) 20–600°C	α (10^{-6} °C^{-1}) 870–1050°C
LSFG 9191	10.1	13.8
LSFG 8291	10.0	16.7
LSFG 7391	10.8	18.0
LSFG 6491	11.9	32.0
LSFG 7373	12.6	22.0
LSFG 6473	11.1	22.5
LSFG 6464	11.0	21.9
LSFG 6482	11.5	22.5

The expansion behaviour, in those two temperature ranges, can be attributed to two different mechanisms. In the low temperature range, typically below 600°C, the intrinsic thermal expansion is due to atomic vibrations of lattice with temperature. In the high temperature range, typically above 870°C, in addition to the intrinsic thermal expansion, another contribution to the volume expansion is caused by oxygen loss from the structure with the creation of oxygen vacancies (reaction 1), commonly called chemical induced expansion. The following reaction, where the Kröger-Vink notation is used, is thermally activated [5,10]:

$$O_O \underset{2}{\overset{1}{\rightleftarrows}} V_O^{\bullet\bullet} + \frac{1}{2}O_2 + 2e' \qquad \textbf{reaction 1}$$

3.2.1 Effects of lanthanum substitution by strontium on TEC

Lanthanum ferrite was doped by strontium in order to improve ionic and electronic conductivities. The ionic conductivity is related to the concentration of oxygen vacancies and the electronic conductivity is related to hole concentration. The partial substitution of lanthanum by strontium can lead to the creation of oxygen vacancies and holes, according to the reactions 2 and 3.

$$2SrO \xrightarrow{LaFeO_3} 2Sr'_{La} + V_O^{\bullet\bullet} + 2O_O^{\times} \qquad \textbf{reaction 2}$$

$$\tfrac{1}{2}O_2 + 2SrO \xrightarrow{LaFeO_3} 2Sr'_{La} + 2h^{\bullet} + 3O_O^{\times}$$

$$Fe_{Fe}^{\times} + h^{\bullet} \rightarrow Fe_{Fe}^{\bullet} \qquad \textbf{reaction 3}$$

$$2Fe_{Fe}^{\times} + V_O^{\bullet\bullet} + \tfrac{1}{2}O_{2(g)} \Leftrightarrow 2Fe_{Fe}^{\bullet} + O_O^{\times} \qquad \textbf{reaction 4}$$

Reaction 4 represents the global equilibrium between reactions 2 and 3 which gives the influence of oxygen partial pressure on the oxygen vacancy concentration. TEC values of perovskites were measured for various strontium contents from LSFG 9191 to LSFG 6491 with a constant gallium content ($La_{(1-X)}Sr_XFe_{0.9}Ga_{0.1}O_{3-\delta}$) under air and nitrogen (Figure 5).

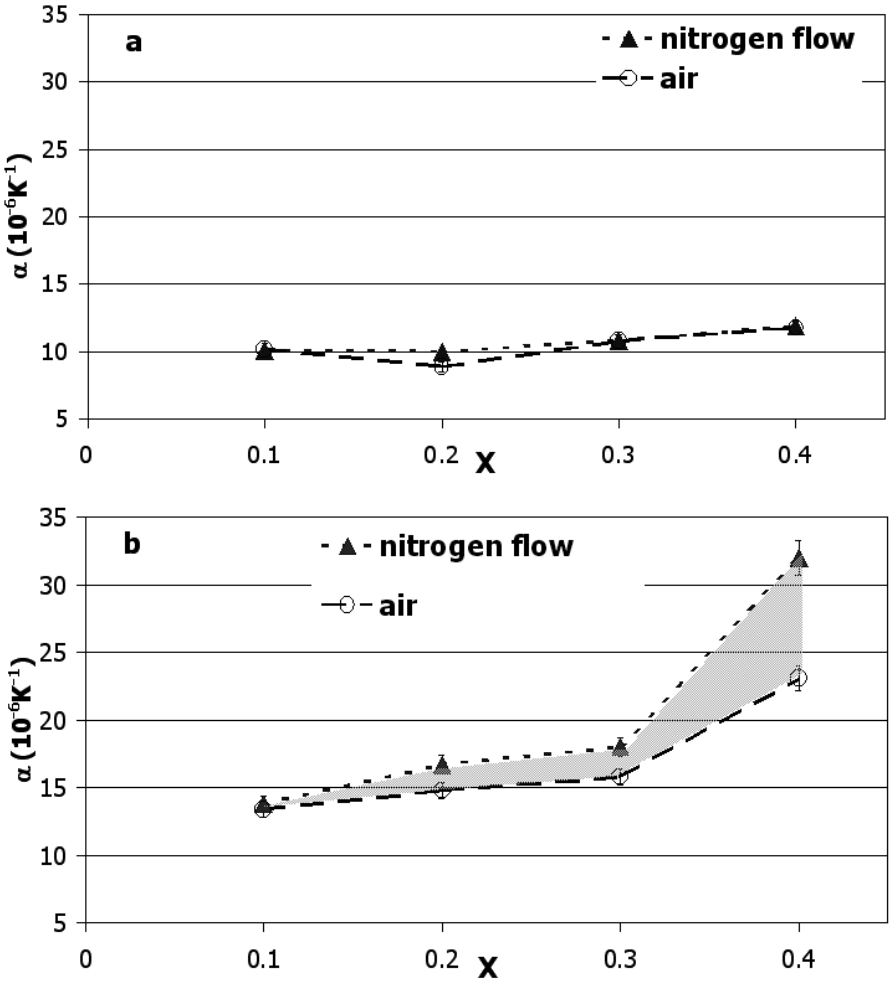

Figure 5 : Variation of the TEC of $La_{(1-X)}Sr_XFe_{0.9}Ga_{0.1}O_{3-\delta}$ with X in air (pO_2 = 0.21) and nitrogen (pO2 = $5x10^{-6}$) for (a): 20 < T < 600°C ; (b): 870 < T < 1050°C.

In the low temperature range, the substitution of lanthanum by strontium from X = 0.1 to 0.4 ($La_{(1-X)}Sr_XFe_{0.9}Ga_{0.1}O_{3-\delta}$) leads to a TEC variation in the range of 8.9 up to 11.9 10^{-6} C^{-1} under air and nitrogen. TEC is slightly affected by strontium content in the low temperature range (Figure 5 a). Indeed in this range, the thermal expansion is only the result of lattice vibrations. In the high temperature range, the TEC increases from 13.4 up to $23.1x10^{-6}°C^{-1}$ in air, and from 13.8 up to $32.0x10^{-6}°C^{-1}$ under nitrogen for strontium content varying from X = 0.1 to 0.4 (Figure 5 b). The difference of TEC between pO_2 = 0.21 atm and $5x10^{-6}$ atm also increases with X values. In the high temperature range, the concentration of oxygen vacancies increases with strontium content (reaction 2) according to the relationship of electroneutrality conservation. The

TEC value is a function of perovskite material oxygen non-stoechiometry (δ) which depends on temperature and oxygen partial pressure. A high level of non-stoechiometry leads to a high expansion intensity. The oxygen non-stoechiometry of the perovskite increases with temperature for a given oxygen partial pressure, and for a given temperature the oxygen non-stoechiometry increases when pO_2 decreases. Mizusaki et al reported this behaviour of oxygen non-stoechiometry for $La_{0.9}Sr_{0.1}FeO_{3-\delta}$ material [12]. Oxygen vacancies created between cations into perovskite structures lead to the increase of the electrostatic repulsion between cations and then also contributes to the volume expansion of the lattice in addition to the lattice vibrations. On the hand, reaction 1 equilibrium is moved in sense 1 [5,7,10] with low pO_2, enhancing the creation of oxygen vacancies in the perovskite structure. On the other hand, reaction 4 involves the creation of oxygen vacancies and the reduction of the valence state of iron from Fe^{4+} ($Fe_{Fe}^{\bullet}$) to Fe^{3+} ($Fe_{Fe}^{\times}$) due to temperature and low oxygen partial pressure. For low pO_2, the volume expansion of the material is due to this reduction of Fe with increasing ionic radii ($r_{Fe}^{4+} = 0.585$ Å; $r_{Fe}^{3+} = 0.645$ Å in coordinance 6 [13]) and to oxygen vacancies with an increase of the electrostatic repulsion between the cations. The result of these chemical-induced mechanisms is a deformation and an increase of the unit cell volume. Over $x = 0.3$, a particular TEC increase was observed. The variation of the TEC between high and low pO_2 is 39% for $X = 0.4$. That is not acceptable in terms of mechanical stability for a CMR.

To minimize the unfavourable expansion caused by the change of ionic iron valence and by the creation of oxygen vacancies, the perovskite B site was substituted by a more stable trivalent cation like Ga^{3+} ($r_{Ga}^{3+} = 0.620$ Å in coordinance 6) [7,13-15].

3.2.2 Effects of iron substitution by gallium on TEC

Using the same approach, the TEC was measured versus Ga content, Sr content remaining constant (i.e. $La_{0.6}Sr_{0.4}Fe_{(1-Y)}Ga_YO_{3-\delta}$, $0.1 \leq Y \leq 0.4$), from LSFG 6491 to LSFG 6464 materials.

In the low temperature range (20–600°C), no significant evolution of TEC values was measured for iron substitution by gallium in the $Y = 0.1$ to 0.4 range (Figure 6 a). Between 870–1050°C, a significant decrease of the TEC value was measured with Ga

content (Figure 6 b). This behaviour mostly appears for low pO_2 (nitrogen). Similar phenomenon was observed by Patrakeev et al [14] on $La_{0.3}Sr_{0.7}Fe_{(1-Y)}Ga_YO_{2.65+\delta}$ perovskites. The Mechanisms are still not well understood. An explanation could be the decrease of Fe concentration as Ga content increases, hence tetravalent iron cation concentration decreases too. Fe substitution by Ga minimizes chemically induced expansion due to Fe^{4+} reduction to Fe^{3+} at low pO_2. Indeed, the Fe^{3+} radius is larger than Fe^{4+} in coordinance 6 [13]. In addition, the concentration of oxygen vacancy, in equilibrium with tetravalent iron cations, is also decreasing. Oxygen vacancies formation and variation of the oxidation state of iron, both depending on temperature and pO_2, have less impact on the unit cell volume [16].

Another assumption is the presence local lattice distortions induced by the substitution of iron cations. Indeed, significant differences exist in the length of Fe-O and Ga-O bonds. The covalent character of the Fe-O bond is lessened with the Ga substitution in perovskite [7]. The Ga-O bond is shorter and stronger than the Fe-O bond [14]. This likely contributes to the variation of unit cell volume with Ga content in perovskite like $La_{(1-X)}Sr_XFe_{(1-Y)}Ga_YO_{3-\delta}$ and then to the TEC variation of.

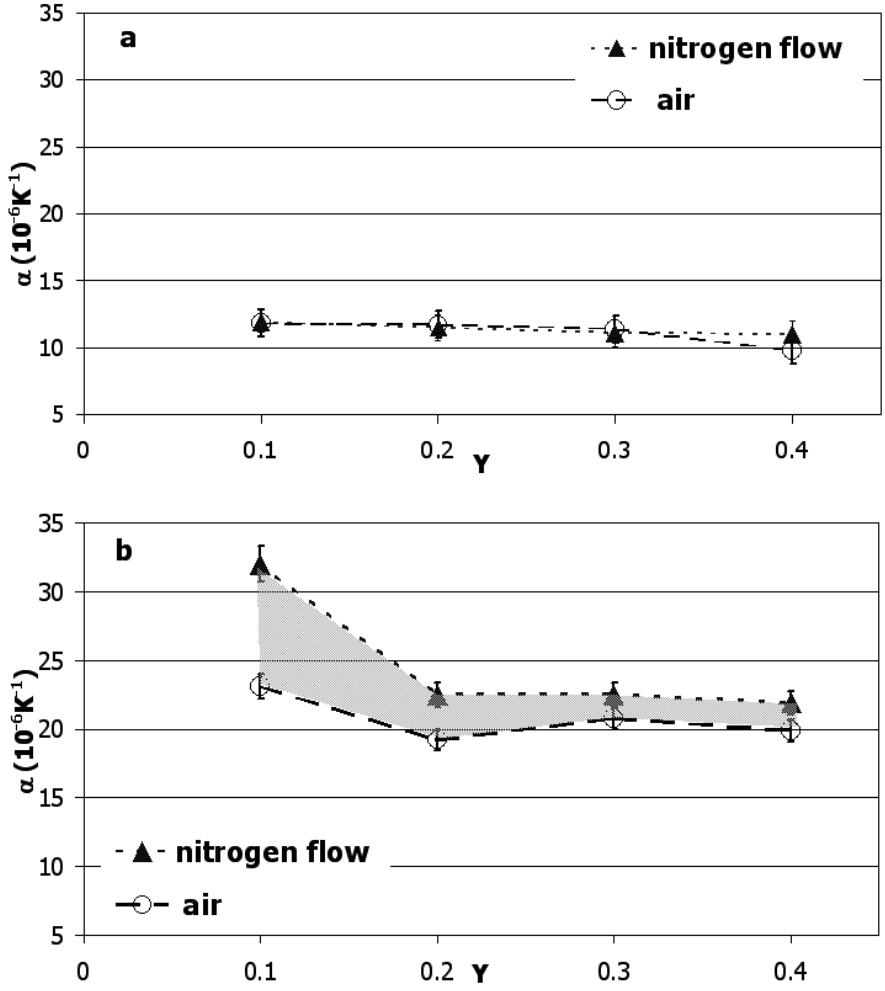

Figure 6 : Variation of the TEC of $La_{0.6}Sr_{0.4}Fe_{(1-Y)}Ga_YO_{3-\delta}$ with Y in air ($pO_2 = 0.21$) and nitrogen ($pO2 = 5x10^{-6}$) for (a) : 20 < T < 600°C ; (b) : 870 < T < 1050°C.

The TEC values measured under air and nitrogen ($pO_2 = 0.21$ and $5x10^{-6}$ atm respectively) for various compositions of $La_{(1-X)}Sr_XFe_{(1-Y)}Ga_YO_{3-\delta}$ materials show an improvement of the dimensional stability with cation substitution. Under those conditions, the smallest difference of TEC values observed between low and high pO_2 were for X = 0.3 and Y = 0.3. In the high temperature range, the variation of α for $La_{0.7}Sr_{0.3}Fe_{0.7}Ga_{0.3}O_{3-\delta}$, between high and low pO_2 is around 16% (Table 2). Nevertheless, under CMR operating conditions, the lowest pO_2 can reach $3x10^{-19}$ atm under methane gas. These results only indicate a tendency of the TEC evolution of the.

Ceramic membranes for catalytic membrane reactor require a high dimensional stability with a high ionic conductivity. Then, a compromise should be found between stability

and oxygen permeation, which requires a sufficient oxygen vacancy amount, then a sufficient Sr content.

3.3 Oxygen permeation

Some studies have shown an influence of membrane microstructures on oxygen permeation fluxes. Kharton et al reported for $LaCoO_{3-\delta}$ [17] and for $SrCo(Fe,Cu)FeO_{3-\delta}$ [18] membranes, an enhancement of oxygen permeation flux with an increase of the average grain size. However other studies reported opposite evolutions of oxygen permeation with microstructure. Diethelm et al. [19] measured a decrease of the ionic conductivity with increasing grain size in a $La_{0.5}Sr_{0.5}FeO_{3-\delta}$ mixed conducting membrane. Etchegoyen et al. [8] measured an enhancement of oxygen permeation flux through a $La_{0.6}Sr_{0.4}Fe_{0.9}Ga_{0.1}O_{3-\delta}$ membrane by a factor 10 at 925°C with the decrease of the average grain size from 3.6 to 1.1 µm. So this present study was performed on similar microstructure membranes to avoid any influence of the microstructure on oxygen flux. Sintering temperatures and dwell times were adjusted to obtain membranes with a relative density higher than 95% and similar grain size distributions (Table 3 and Figure 7).

Table 3: Mean grain size and relative density of four materials membrane for different sintering conditions.

Compositions	Sintering temperature (°C)	Dwell time (h)	Average grain size (µm)	Relative density (%)
LSFG 6491	1250	5	0.90	98.9
LSFG 6464	1300	2	0.91	99.0
LSFG 9191	1300	6	0.80	97.8
LSFG 7373	1350	9	1.06	99.0

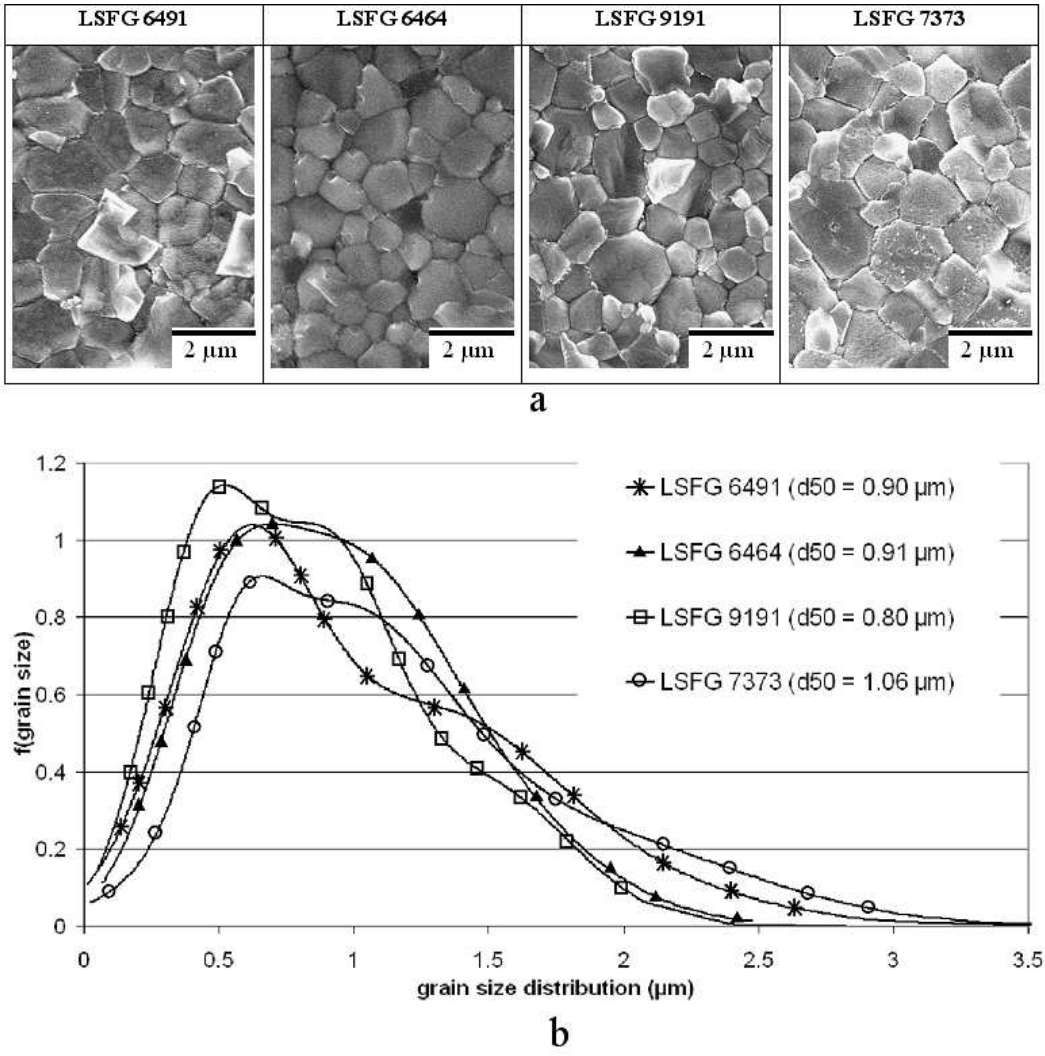

Figure 7 : LSFG 6491, LSFG 6464, LSFG 9191 and LSFG 7373 dense membranes sintered under conditions given in table 3; (a) : microstructures (SEM); (b) : grain size distributions (image analysis).

Oxygen permeation through LSFG 9191, LSFG 6464, LSFG 7373 and LSFG 6491 dense membranes, was measured in the 750 to 975°C temperature range (Figure 8). The increase of the oxygen flux with temperature is due to higher mobility and concentration of ionic carriers [20,21]. Below 850°C, oxygen permeation fluxes are low and similar for all the membranes. LSFG 6491 and LSFG 6464 membranes present similar oxygen permeation performances in the temperature range tested. At 980°C, LSFG 9191 permeation is about 2.5 times lower than for LSFG 6491 and LSFG 6464 membranes. Oxygen flux measured on LSFG 9191 membranes is lower than the three other membranes. LSFG 7373 dense membranes give intermediate performance. Those

results suggest that a high substitution of La by Sr , such as in LSFG 6491 or LSFG 6464, i.e. materials with a high oxygen vacancy content, improves oxygen permeation flux across a dense membrane.

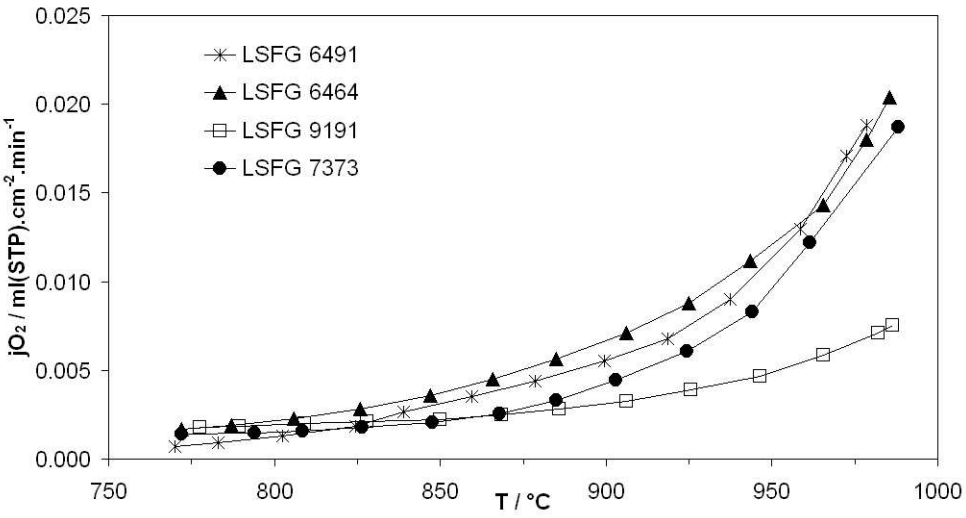

Figure 8 : Evolution of oxygen permeation flux through LSFG membranes with temperature and for different cation substitutions.

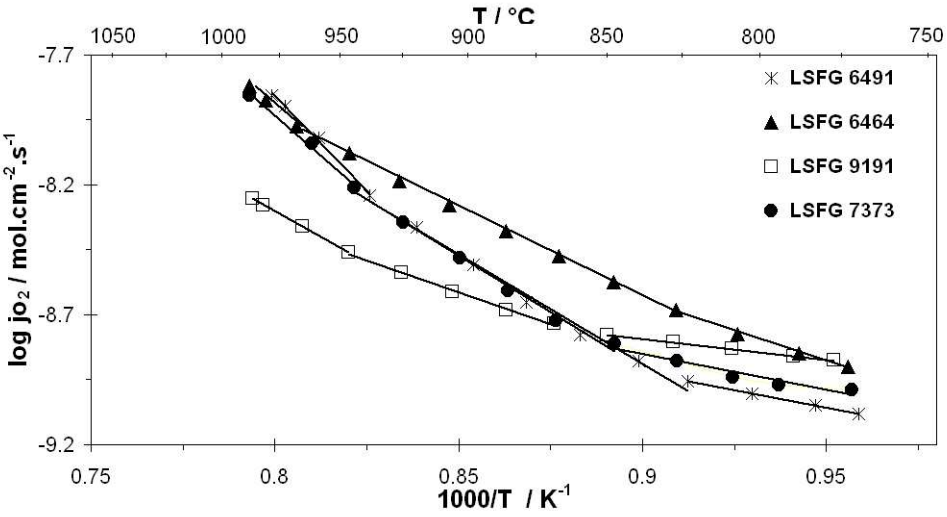

Figure 9 : Arrhenius plots of oxygen permeation fluxes across LSFG 6491, LSFG 6464, LSFG 9191 and LSFG 7373 membranes with an equivalent microstructure.

Table 4: Activation energies of different compositions for the three temperature range.

Compositions	Ea ($kJ.mol^{-1}$)		
	Ea1	**Ea2**	**Ea3**
LSFG 6491	51	161	279
LSFG 6464	89	135	230
LSFG 9191	35	102	151
LSFG 7373	55	170	255

Oxygen transport across a dense membrane is thermally activated according to Arrhenius' law (Figure 9 and Table 4). A lot of mixed oxides present an Arrhenius plot with two slopes like $La_{0.5}Sr_{0.5}FeO_{3-\delta}$ [19] or $(La_{0.9}Sr_{0.1})(Ga_{1-x}Ni_x)_{0.8}Mg_{0.2}O_{3-y}$ with x = 0.25 and x = 0.3 [22]. For all the tested membranes, three slopes can be observed over the temperature range; those slopes changes are reversible with temperature cycling. The lowest temperature slope break in the Arrhenius plot, around 825°C, could be explained by the creation of oxygen vacancies. That can be confirmed by the chemical expansion observed above 800°C (Figure 4), suggesting that the physical phenomena at the origin of Arrhenius and dilatometric breaking lines are similar. At higher temperatures around 950°C, the second break in the Arrhenius plot could be explained by a change with temperature of the rate-controlling mechanism of oxygen transport through the dense membrane, such as surface exchange or bulk diffusion [20,23]. Additional analysis and studies are needed to clarify the rate-limiting mechanism. Investigation methods could be oxygen permeation measurement through a perovskite membrane, with a surface modified by a catalytic layer and/or oxygen activity measurement of dense membrane surfaces. As reported by Guillodo et al. [24], this latter characterization method uses a zirconia tip electrode in contact with the surface of the dense membrane to evaluate respective contributions of oxygen surface exchange and bulk oxygen diffusion.

Performances reported on the same or similar materials are better than results obtained on our membranes and can differ by more than one order of magnitude. The Oxygen permeation flux of our materials $(La_{(1-X)}Sr_XFe_{(1-Y)}Ga_YO_{3-\delta}$ with $0<X\leq0.4$ and $0<Y\leq0.4$),

at 900°C are between 0.003 and 0.007 ml(STP).cm^{-2}.min^{-1} with a membrane thickness around 1 mm. Indeed, according to Wargner's theory the oxygen flux permeating across a dense membrane can be significantly affected by the thickness of the membrane [9,17]. For comparison, Lee et al [20] measured around 900°C an oxygen permeation flux of about 0.025 ml(STP).cm^{-2}.min^{-1} for $La_{0.7}Sr_{0.3}Fe_{0.4}Ga_{0.6}O_{3-\delta}$ and 0.15 ml(STP).cm^{-2}.min^{-1} for $La_{0.6}Sr_{0.4}Co_{0.2}Fe_{0.8}O_{3-\delta}$ with a 1.7 mm membrane thickness. Teraoka et al. [25] measured around 900°C an oxygen permeation flux of about 1.1 ml(STP).cm^{-2}.min^{-1} for $La_{0.2}Sr_{0.8}Co_{0.8}Fe_{0.2}O_{3-\delta}$ with a 1 mm membrane thickness. We have to keep in mind that a high oxygen permeation requires a high oxygen vacancy content, i.e. high oxygen non-stoechiometry, and corresponds to materials with a low chemical and dimensional stability, as explained in section 3.2 [26].

This study shows that a good compromise seems to be found with $La_{0.7}Sr_{0.3}Fe_{0.7}Ga_{0.3}O_{3-\delta}$ materials, likely with an intermediate oxygen permeation flux, but with a low TEC difference under studied conditions.

4. Conclusion

Dense $La_{(1-X)}Sr_XFe_{(1-Y)}Ga_YO_{3-\delta}$ (with $0<X\leq0.4$ and $0<Y\leq0.4$) materials were prepared from powder synthesized by a classic solid state reaction route. They were characterized by X-ray diffraction, dilatometry and oxygen permeation flux measurements. Increasing strontium content and iron content in LSFG materials induces an evolution of crystal symmetry and an expansion of the unit cell volume. Sr content and oxygen vacancy concentration in the material are linked and affect expansion behaviour mainly above 870°C. At high temperature the TEC increases with oxygen vacancy concentration and with the decrease of pO_2. Fe substitution by Ga cations has an interesting influence on TEC. A dimensional stabilisation is induced by gallium addition in the $La_{(1-X)}Sr_XFe_{(1-Y)}Ga_YO_{3-\delta}$ material for substitution values (Y) larger than 0.2.

Concerning oxygen permeation, Ga cation concentration has no significant effect. Sr content has a beneficial effect, due to creation of oxygen vacancies. In the composition field studied, LSFG 7373 seems to be the best compromise between performance and dimensional stability. The two breaks in the Arrhenius plots of oxygen permeation suggest the presence of three limiting steps in oxygen permeation across membranes. The first slope may be attributed to the creation of oxygen vacancies. The interpretation of the two others, at higher temperatures, requires additional analysis to clarify the rate-limiting mechanisms which control oxygen permeation through the membrane. Investigation methods like oxygen surface activity measurement using a zirconia tip electrode could give information on the respective contribution of oxygen surface exchange and bulk diffusion.

Acknowledgements

The authors wish to express their gratitude to Air Liquide and CNRS for technical and financial support and ADEME (French environment and energy management agency) for financial support of this Study.

References

[1] A.F. Sammells, M. Schwartz, R.A. Mackay, T.F. Atmton, D.R. Peterson, Catalytic membrane reactors for spontaneous synthesis gas production, Catalysis Today, 56 (2000) 325.

[2] U. Balachandran, J.T. Dusek, R.L. Mieville, R.B. Poeppel, M.S. Kleefisch, S. Pei, T.P. Kobylinski, C.A. Udovich, A.C. Bose, Dense ceramic membranes for partial oxidation of methane to syngas, Applied Catalysis A: General, 133 (1995) 19.

[3] H.J.M. Bouwmeester, Dense ceramic membranes for methane conversion, Catalysis Today, 82 (2003) 141.

[4] Y. Teraoka, H. M. Zhang, S. Furukawa, N. Yamazoe, oxygen permeation through perovskite-type oxides, Chemistry Letters, (1985) 1783.

[5] V.V. Kharton, A.A. Yaremchenko, M.V. Patrakeev, E.N. Naumovich, F.M.B. Marques, Thermal and chemical induced expansion of $La_{0.3}Sr_{0.7}(Fe,Ga)O_{3-\delta}$ ceramics, J. Eur. Ceram. Soc., 23 (2003) 1417.

[6] M.A. Pena, J.L.G. Fierro, Chemical Structures and Performance of Perovskite Oxides, Chem. Rev., 101 (2001) 1981.

[7] V.V. Kharton, A.L. Shaulo, A.P. Viskup, M. Avdeev, A.A. Yaremchenko, M.V. Patrakeev, A.I. Kurbakov, E.N. Naumovich, F.M.B. Marques, Perovskite-like system $(Sr,La)(Fe,Ga)O_{3-\delta}$: structure and ionic transport under oxidizing conditions, Solide State Ionics, 150 (2002) 229.

[8] G. Etchegoyen, T. Chartier, A. Julian, P. Del-Gallo, Microstructure and oxygen permeability of a $La_{0.6}Sr_{0.4}Fe_{0.9}Ga_{0.1}O_{3-\delta}$ membrane containing magnesia as dispersed second phase particles, Journal of Membrane Science, 268 (2006) 86.

[9] G. Etchegoyen, T. Chartier, P. Del-Gallo, An architectural approach to the oxygen permeability of a $La_{0.6}Sr_{0.4}Fe_{0.9}Ga_{0.1}O_{3-\delta}$ perovskite membrane, J. Eur. Ceram. Soc., 26 (2006) 2807.

[10] H. Ullmann, N. Trofimenko, F. Tietz, D. Stover, A. Ahmad-Khanlou, Correlation between thermal expansion and oxide ion transport in mixed conducting perovskite-type oxides for SOFC cathodes, Sol St Ion, 138 (2000) 79.

[11] C.Y. Park, A.J. Jacobson, Thermal and chemical expansion properties of $La_{0.2}Sr_{0.8}Fe_{0.55}Ti_{0.45}O_{3-x}$, Sol St Ion, 176 (2005) 2671.

[12] J. Mizusaki, M. Yoshihiro, S. Yamauchi, K. Fueki, Nonstoichiometry and defect structure of the perovskite-type oxides $La_{1-x}Sr_xFeO_{3-\circ}$, Journal of Solid State Chemistry, 58 (1985) 257.

[13] R.D. Shannon, Revised effective ionic radii and systematic studies of interatomic distances in halides and chalcogenides, Acta Crystallographica, Section A (Crystal Physics, Diffraction, Theoretical and General Crystallography), A32, Part 5 (1976) 751.

[14] M.V. Patrakeev, E.B. Mitberg, A.A. Lakhtin, I.A. Leonidov, V.L. Kozhevnikov, V.V. Kharton, M. Avdeev, F.M.B. Marques, Oxygen Nonstoichiometry, Conductivity, and Seebeck Coefficient of $La_{0.3}Sr0.7Fe_{1-x}Ga_xO_{2.65+\delta}$ Perovskites, Journal of Solid State Chemistry, 167 (2002) 203.

[15] H. Wang, W.S. Yang, Y. Cong, X. Zhu, Y.S. Lin, Structure and oxygen permeability of a dual-phase membrane, Journal of Membrane Science, 224 (2003) 107.
[16] D. Kuscer, D. Hanzel, J. Holc, M. Hrovat, D. Kolar, Defect structure and electrical properties of $La_{1-y}Sr_yFe_{1-x}Al_xO_{3-\delta}$, J. Am. Ceram. Soc., 84 (2001) 1148.
[17] V.V. Kharton, E.N. Naumovich, A.V. Kovalevsky, A.P. Viskup, F.M. Figueiredo, I.A. Bashmakov, F.M.B. Marques, Mixed electronic and ionic conductivity of $LaCo(M)O_3$ (M=Ga, Cr, Fe or Ni): IV. Effect of preparation method on oxygen transport in $LaCoO_{3-\delta}$, Solid State Ionics, 138 (2000) 135.
[18] V.V. Kharton, V.N. Tikhonovich, L. Shuangbao, E.N. Naumovich, A.V. Kovalevsky, A.P. Viskup, I.A. Bashmakov, A.A. Yaremchenko, Ceramic microstructure and oxygen permeability of $SrCo(Fe, M)O_{3-\delta}$(M = Cu or Cr) perovskite membranes, J. Electrochem. Soc., 145 (1998) 1363.
[19] S. Diethelm, J. Van herle, J. Sfeir, P. Buffat, Correlation between oxygen transport properties and microstructure in $La_{0.5}Sr_{0.5}FeO_{3-\delta}$, Journal of the European Ceramic Society, 25 (2005) 2191.
[20] Lee, K.S. Lee, S.K. Woo, J.W. Kim, T. Ishihara, D.K. Kim, Oxygen-permeating property of $LaSrBFeO_3$ (B=Co, Ga) perovskite membrane surface-modified by $LaSrCoO_3$, Solid State Ionics, 158 (2003) 287.
[21] J.-M. Kim, G.-J. Hwang, S.-H. Lee, C.-S. Park, J.-W. Kim, Y.-H. Kim, Properties of oxygen permeation and partial oxidation of methane in $La_{0.6}Sr_{0.4}CoO_{3-\delta}$ (LSC)-$La_{0.7}Sr_{0.3}Ga_{0.6}Fe_{0.4}O_{3-\delta}$ (LSGF) membrane, Journal of Membrane Science, 250 (2005) 11.
[22] E.D. Politova, V.V. Aleksandrovskii, G.M. Kaleva, A.V. Mosunov, S.V. Suvorkin, S.V. Zaitsev, J.S. Sung, K.Y. Choo, T.H. Kim, Mixed conducting perovskite-like ceramics on the base of lanthanum gallate, Solid State Ionics, 177 (2006) 1779.
[23] S.J. Xu, W.J. Thomson, Oxygen permeation rates through ion-conducting perovskite membranes, Chemical Engineering Science, 54 (1999) 3839.
[24] M. Guillodo, J. Foulrtier, L. Dessemond, P.D. Gallo, Oxygen permeation through dense $Bi_2V_{0.9}Cu_{0.1}O_{5.35}$ ceramic membranes, Journal of the Electrochemical Society, 149 (2002) 93.
[25] Y. Teraoka, Y. Honbe, J. Ishii, H. Furukawa, I. Moriguchi, Catalytic effects in oxygen permeation through mixed-conductive LSCF perovskite membranes, Solid State Ionics, 152-153 (2002) 681.
[26] I. Kaus, K. Wiik, K. Kleveland, B. Krogh, S. Aasland, Oxygen transport properties in $La_{1-x}Sr_xFe_{1-y}M_yO_{3-\delta}$ (M = Cr, Ti), $0.2 < x < 0.8$, $0.2 < y_{Ti} < 0.5$, $0.1 < y_{Cr} < 0.3$, Solid State Ionics, 178 (2007) 817.

Figure 8: Evolution of oxygen permeation flux through LSFG membranes with temperature and for different cation substitutions.

Figure 9: Arrhenius plots of oxygen permeation fluxes across LSFG 6491, LSFG 6464, LSFG 9191 and LSFG 7373 membranes with an equivalent microstructure.